THE JOURNAL OF PHYSICAL CHEMISTRY B

Article

pubs.acs.org/JPCB

Energetics of Mutation-Induced Changes in Potency of Lersivirine against HIV-1 Reverse Transcriptase

Parimal Kar and Volker Knecht*

Department of Theory and Bio-Systems, Max Planck Institute of Colloids and Interfaces, Am Mühlenberg 1, 14476 Potsdam, Germany

Supporting Information

ABSTRACT: Nonnucleoside reverse transcriptase inhibitors (NNRTIs) are key components of highly active antiretroviral therapy for the treatment of HIV-1. A common problem with the first generation NNRTIs is the emergence of mutations in the HIV-1 reverse transcriptase (RT), in particular, K103N and Y181C, which lead to resistance to the entire class of inhibitor. Here we have evaluated the relative affinity of the newly designed NNRTI lersivirine (LRV) against drug-resistant mutations in HIV-1 RT using the molecular mechanics generalized Born surface area (MM-GBSA) method. Eight single and one double mutant variants of RT are considered. Our results are in good agreement with experimental results and yield insights into the mechanisms underlying mutation-induced changes in the potency of LRV against RT. The strongest (54-fold) increase in the dissociation constant is found for the mutant F227C, originating from reduced electrostatic and van der Waals interactions between LRV and RT as well as a higher energetic penalty from the desolvation of polar groups. For the mutants K103N and Y181C only a moderate (2-fold) increase in the dissociation constant is found, due to a balance of opposite changes in the polar solvation as well as the electrostatic and van der Waals interactions between LRV and RT. The dissociation constant is decreased for the Y188C and G190A (2-fold), the M184V (5-fold), and the Y188C/Y188C mutant (10-fold), due to stronger electrostatic interactions between LRV and RT. Our results thus suggest that LRV is a highly potent and selective NNRTI, with excellent efficacy against NNRTI-resistant viruses, which is in agreement with experimental observations.

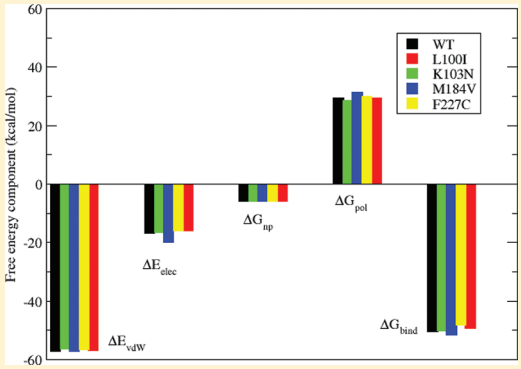

1. INTRODUCTION

The acquired immune deficiency syndrome (AIDS) was first reported in 1981, and since then, it has rapidly developed into a pandemic fatal disease. According to the UNAIDS 2009 report, approximately 60 million people worldwide have been infected with AIDS, with 25 million deaths.[1] AIDS is caused by the human immunodeficiency virus (HIV). To date, no cure exists to eliminate HIV.

Reverse transcriptase (RT) is a key enzyme in the replication cycle of the human immunodeficiency virus type 1 (HIV-1), catalyzing the conversion of virally encoded single-stranded RNA (ribonucleic acid) into proviral double-stranded DNA (deoxyribonucleic acid), which is subsequently integrated into the host cell genome by an integrase enzyme.[2,3] This essential step in the retroviral life cycle is targeted by a variety of drugs in clinical use to combat AIDS. The RT enzyme contains two main domains: a DNA polymerase domain which is able to copy either an RNA or DNA template and a ribonuclease H (RNase H) domain whose function is to cleave and degrade the template RNA after DNA synthesis so that the newly made DNA can generate a second DNA strand.

RT (shown in Figure 1) is a heterodimeric enzyme composed of two distinct, but related chains, a 66 kD subunit (p66) composed of 560 amino acids and 51 kD subunit (p51) comprising 440 amino acids.[4] The p66 subunit (blue in Figure 1) consists of "fingers" (amino acids 1−85 and 118−155), a "palm" (amino acids 86−117 and 156−237), and a "thumb" subdomain (amino acids 238−318), as well as a connection (amino acids 319−426) and a ribonuclease H (RNase H) subdomain (amino acids 427−560). The p51 subunit also contains the finger, palm, thumb, and the connection subdomains but not the C-terminal RNase domain present in p66. The first 440 amino acid residues in the p66 subunit are the same as in the p51 subunit. Despite their sequence homology, a flexible and open structure is assumed by the p66 subunit, whereas "the p51 subunit is rather compact, and seems to play a structural role, devoid of catalytic activity, with the three aspartic acids buried inside".[4,5] New DNA is synthesized between the cleft of the thumb and the fingers subdomain while a viral RNA strand is held in place as a template.[6]

RT is essential for viral replication. The polymerase of HIV-1 RT is a major target for anti-HIV-1 drugs. With the introduction of highly active antiretroviral drugs, the treatment of AIDS patients has been improved, effectively decreasing the

Received: January 25, 2012
Revised: May 8, 2012
Published: May 10, 2012

dx.doi.org/10.1021/jp300818c | J. Phys. Chem. B 2012, 116, 6269−6278

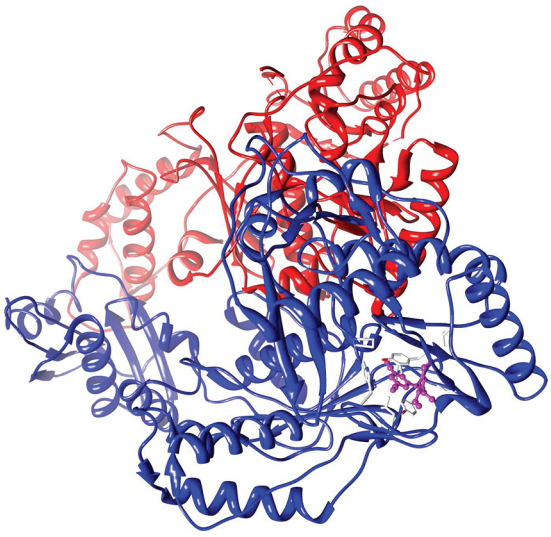

Figure 1. Crystal structure of the HIV-1 RT_{WT}–LRV complex. The inhibitor LRV is shown as magenta balls and sticks. The protein is shown in the ribbon representation; the p51 and p66 subunits are colored red and blue, respectively.

mortality rate of HIV/AIDS patients.[7] Developing vaccines to fight the AIDS infection is challenging.[8] The treatment of care is known as highly active antiretroviral therapy (HAART). This treatment consists of a combination of at least three selected antiretroviral drugs (taken from six different drug classes) that inhibit (i) the HIV replication cycle at the point of entry (chemokine antagonists and fusion inhibitors), (ii) reverse transcription (nucleoside/nucleotide and nonnucleoside RT inhibitors), and (iii) integration (integrase inhibitors), or viral production (protease inhibitors).[9]

There are two main classes of RT inhibitors. The first class consists of nucleoside analogues (known as nucleoside reverse transcriptase inhibitors, or NRTIs) such as AZT or atazanavir (3′-azido-3′-deoxythymidine), ddC (dideoxycytidine), and so forth. The nucleoside analogue lacks a hydroxyl group and cannot react with the nucleoside any more, preventing DNA elongation. The second class consists of nonnucleoside reverse transcriptase inhibitors (NNRTIs) such as HEPT (1-[(2-hydroxyethoxy)-methyl]-6-(phenylthio)thymine),[10] TIBO (tetrahydroimidazo-[4,5,1-*jk*][1,4]-benzo diazepin-2(1*H*)-one),[11] nevirapine (dipyridodiaze pinones),[12] efavirenz ((−)-6-chloro-4-cyclopropyl ethynyl-4-trifluoromethyl-1,4-dihydro-2*H*-3,1-benzoxazin-2-one),[13] and delavirdine.[14] The NNRTIs bind at an allosteric site on the p66 subdomain, known as the nonnucleoside binding pocket (NNBP).[15] The allosteric mode of action of inhibitors against HIV-1 RT is discussed elsewhere.[16] The direct comparison the of apo and NNRTI-bound RT structure in similar crystal form delineates the conformational changes required to form the NNRTI site. It has been observed that the NNRTIs achieve specificity not simply by filling an arbitrary pocket but rather by emulating the protein–protein interactions that stabilize the structure of the inactive p51, resulting in a distortion of the polymerase active-site by movement of the key aspartic acid residues, and hence a common mechanism of inhibition by this diverse class of HIV-1 specific RT inhibitors.[16] All of these NNRTIs are effective in inhibiting HIV replication, but their use and compliance are limited by serious side effects, frequently leading to the rapid generation of resistance through single point mutations which can lead to class resistance.[9,17] These are first-generation NNRTIs. Second-generation NNRTIs, which are either licensed or in clinical development, retain activity against clinically significant drug-resistive mutant variants of HIV-1 RT. Etravirine (TMC-125) is one of such second-generation NNRTIs whose efficacy in treatment-naïve patients remains to be established.

In this work, we have studied the binding of the RT inhibitor lersivirine (LRV), also called UK-453061, to the wild-type RT and mutant variants. LRV is a second-generation drug and in a preclinical stage now. The binding pocket of the HIV-1 RT–LRV complex is shown in Figure 2, and the chemical structure

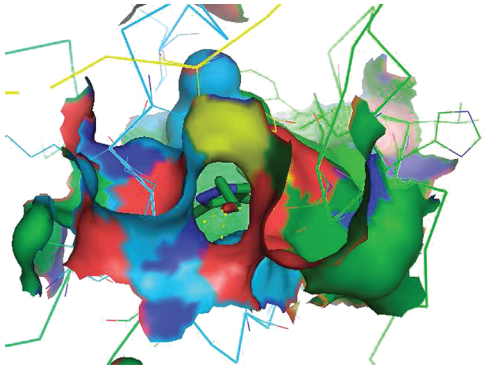

Figure 2. Binding pocket of the HIV-1 RT_{WT}–LRV complex with hydrogen bonds shown as dotted yellow lines. The ligand is depicted as sticks, the protein as solid lines and as a surface (around the binding pocket). For the ligand, colors distinguish between carbon (green), oxygen (red), and nitrogen (blue). For the protein, colors distinguish between individual amino acid residues.

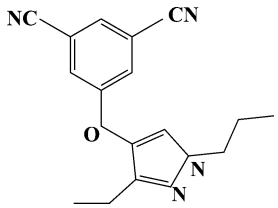

Figure 3. Chemical structure of lersivirine.

of LRV is shown in Figure 3. This drug was synthesized by Corbau et al.[9] and resulted from lead optimization of a substituted pyrazole. Preclinical data[9] suggest that LRV inhibits clinically relevant viral strains. This drug is active in primary blood cell assays and against viruses of different clades and diverse geographical origins.[9] Experiments performed using a cytopathic-effect-based assay with HIV-1 NL4-3 in MT-2 cells suggest that LRV is also additive or synergistic with other antiretroviral agents.[9] Combinations of LRV with drugs of the NRTI class (abacavir, didanosine, emtricitabine, lamivudine, tenofovir, and zidovudine) resulted in synergistic interactions. In addition, Corbau et al. have observed synergistic interactions with the integrase inhibitors elvitegravir and raltegravir and the fusion inhibitor enfuvirtide. Additive interactions were observed when LRV was used in combination with a protease inhibitor (atazanavir, lopinavir, and ritonavir). It has been shown in vitro that it inhibits the RT enzyme by a mixed noncompetitive kinetic mechanism and binds the protein with a 1:1 stoichiometry in the NNRTI binding pocket. X-ray crystallog-

dx.doi.org/10.1021/jp300818c | *J. Phys. Chem. B* 2012, 116, 6269–6278

raphy suggests a novel binding mode of LRV into the "NNRTI pocket", which in turn translates to activity against key class resistance mutants.[9]

The X-ray structure confirmed that LRV binds noncovalently to the allosteric, nonnucleoside binding site of recombinant WT HIV-1 RT. Detailed analysis of this binding indicates that LRV forms interactions with residues L100, V106, Y181C, Y188, F227, W229, L234, P236, and Y318 of the p66 subunit of RT. V108 forms extensive van der Waals interactions with the dicyano-substituted phenol moiety of LRV. In addition, LRV forms three hydrogen bonds with residues Lys103 and Pro236.

To elucidate the mechanism underlying the binding of LRV to wild-type RT and its mutant variants from an energetic point of view, we have used molecular dynamics simulations and free energy calculations to study the contributions to the binding affinities for the respective complexes. The most rigorous and accurate methods to calculate binding free energies are free energy perturbation[18] and thermodynamic integration.[19] Here, the sum of small free energy changes along a physical or alchemical multistep pathway connecting the bound and the unbound state is evaluated. However, these methods are computationally very expensive. In contrast, generating conformational ensembles for the free and the bound species and evaluating the corresponding free energies using the molecular mechanics-Poisson−Boltzmann or generalized Born surface area (MM-PB/GBSA) methods[20−22] is faster by several orders of magnitude than free energy perturbation or thermodynamic integration. The PB model is theoretically more rigorous than the GB model, and MM-PBSA is often considered to be naturally superior to MM-GBSA for predicting absolute binding free energies. The GB parameters are usually chosen to match experimental solvation free energies.[23,24] The prediction errors of GB can be well reduced by defining more atom types. A recent study by Hou and co-workers,[25] however, shows that, although MM-GBSA achieves worse predictions for the absolute binding free energies than MM-PBSA, it shows a better performance in ranking the binding affinities for systems without metals. As the focus of our work is to predict the ranking due to single point mutations, MM-GBSA thus even appears to be more useful than MM-PBSA for the current study.

In MM-GBSA methods, the binding free energy is estimated as an average of molecular mechanical energies and solvation free energies of an ensemble of configurations of the molecular complex obtained from a trajectory of a molecular dynamics simulation in explicit water. The MM-GBSA methods have successfully been used to estimate the binding free energy of protein−ligand[26,27] and protein-RNA[28,29] associations. This method has also been used previously to study the binding of different inhibitors to HIV-1 RT.[2,30] Recently Worch et al.[31] have modeled the interaction propensity of transmembrane domain (TMD) pairs and computed free energy gain for TMD dimer formation using the MM-PBSA approach. Compared to our protocol, the PBSA term was replaced with a multiple continuum approach established to mimic biomembrane environments with the aqueous phase being modeled by water, the polar headgroup region by ethanol, and the hydrophobic core by cyclohexane.[32] Generally, the entropic contribution is obtained from a normal-mode analysis (NMA)[33,34] of the complex and the individual binding partners. However, in our current work the contribution from the change in entropy of the binding partners was not determined. The relative binding constants agree well with the experimental data, supporting the notion that the entropy contribution cancels out in relative binding free energies and relative binding constants.[35] A decomposition of the binding free energy into various components yields insights into the origins of mutation-induced affinity changes and, thus, the mechanism of drug resistance or enhanced potency.

2. MATERIALS AND METHODS

2.1. Structure Generation with Periodic Boundary MD Simulations in Explicit Water. The initial coordinates for our simulations were obtained from X-ray crystallographic structures of the HIV-1 RT complexed with the drug LRV. Corbau and co-workers[9] have determined X-ray crystallographic structures of the wild-type HIV-1 RT and the K103N mutant variant complexed with LRV at resolutions of 2.80 Å and 3.20 Å, respectively. The atomic coordinates with the Protein Data Bank accession code 2WON for wild-type HIV-1 RT_{WT}−LRV and 2WOM for RT_{K103N}−LRV were used for our current study. We have also investigated the activity of this drug against other single mutant variants of RT, such as L100I, K101E, Y181C, M184V, Y188C, G190A, F227C, F227L, and the Y181C/Y188C double mutant. The initial configurations of these mutants were derived from the X-ray crystallographic structure of the wild-type HIV-1 RT.

The proteins were described using the Amber ff99SB force field.[36] The ligand was assigned generalized Amber force field (GAFF)[37] atom types, and AM1-BCC[38] atomic charges were calculated with the *antechamber*[39] module of Amber.[40] The AM1-BCC charge for an atom is obtained by adding the bond charge correction (BCC) to a semiempirical quantum calculation of the molecular electronic structure according to the Austin Model 1 (AM1) population atomic charge.[41] It has been shown that atomic charges obtained from this charge model emulate the HF/6-31G* electrostatic potential at the surface of a molecule.[38] Our previous works[42−45] show that this charge scheme is suitable for this kind of studies.

The configurations were generated via simulations of the complexes in explicit water. To this aim, the complex was solvated in TIP3P[46] water using a truncated octahedron periodic box extending at least 10 Å from the complex. Nearly 38 830 water molecules were added to solvate the complex, and the resulting box size was nearly 142.5 Å × 142.5 Å × 142.5 Å. An appropriate number of chloride ions were added to the system to neutralize the charge of the system. All bond lengths involving hydrogen atoms were constrained using the SHAKE[47] algorithm allowing the usage of a 2 fs time-step. The temperature was kept fixed at 300 K using a Langevin thermostat with a collision frequency of 2 ps^{-1}. The electrostatics were treated using the particle-mesh Ewald (PME)[48] scheme with a fourth-order B-spline interpolation and a tolerance of 10^{-5}. The nonbonded cutoff was 8 Å, and the nonbonded pair list was updated every 50 fs.

The simulations were conducted according to the following protocol: (i) the complex was first optimized by 500 steps of steepest descent followed by another 500 steps of conjugate gradient minimization, keeping all atoms of the complex restrained to their initial position with a weak harmonic restraint. (ii) After the minimization, a 50 ps MD simulation at constant volume and 300 K with a 2 $kcal{\cdot}mol^{-1}{\cdot}Å^{-2}$ restraint on the complex was performed to equilibrate the solvent without undesirable drifts in the structure. (iii) Next, a 50 ps MD simulation with a 2 $kcal{\cdot}mol^{-1}{\cdot}Å^{-2}$ restraint on the complex was carried out at a pressure of 1 atm to equilibrate the density

dx.doi.org/10.1021/jp300818c | J. Phys. Chem. B 2012, 116, 6269−6278

using Berendsen's barostat. (iv) Then, the complex was equilibrated for 1 ns without restraint. After the equilibration phase, a 5 ns simulation at constant pressure was conducted, and the coordinates were saved in every 10 ps, resulting in 500 configurations for each simulation. However, only the final 300 configurations were used for estimating the binding free energy.

2.2. MM-GBSA Calculations. The RT-inhibitor (P−I) complex formation reaction is represented by the scheme

$$[\mathrm{P}]_{aq} + [\mathrm{I}]_{aq} \leftrightarrow [\mathrm{PI}]_{aq} \tag{1}$$

where all of the reactants are assumed to be in aqueous solution. The binding affinity is determined from the free energies of the receptor/protease (P), the ligand/inhibitor (I), and the complex (PI), according to

$$\Delta G_{bind} = G_{PI} - (G_P + G_I) \tag{2}$$

In MM-GBSA calculations, the free energy of each species (P, I, PI) is estimated from

$$G = \langle E_{MM} \rangle + \langle G_{pol} \rangle + \langle G_{np} \rangle - T\langle S_{MM} \rangle \tag{3}$$

Here, E_{MM} is the molecular mechanics (MM) gas-phase energy of the species, G_{pol} is the polar contribution to the solvation free energy of the species, estimated from the solution of the generalized Born equation, G_{np} is the nonpolar solvation free energy, T is the absolute temperature of the system, and S_{MM} is the entropy of the species. The gas-phase MM energy E_{MM} can be expressed as

$$E_{MM} = E_{cov} + E_{elec} + E_{vdW} \tag{4}$$

where E_{cov}, E_{elec}, and E_{vdW} denote the contributions from covalent, electrostatic, and van der Waals interactions, respectively. The covalent or bonded contribution includes terms representing bond stretching (E_{bond}), angle vibrational (E_{angle}), and dihedral angle torsion energies ($E_{dihedral}$), according to

$$E_{cov} = E_{bond} + E_{angle} + E_{dihedral} \tag{5}$$

The entropy S_{MM} is composed of a translational (S_{trans}), a rotational (S_{rot}), and a vibrational (S_{vib}) contribution according to

$$S_{MM} = S_{trans} + S_{rot} + S_{vib} \tag{6}$$

The vibrational contribution is determined from a normal-mode analysis of selected configurations at the MM level. The nonpolar solvation term (G_{np}) was estimated from[49]

$$G_{np} = \gamma A + b \tag{7}$$

with γ = 0.00542 kcal·mol^{-1}·Å^{-2} and b = 0.92 kcal·mol^{-1}. The symbol A denotes the solvent accessible surface area (SASA) of the species for a given configuration. The SASA was determined with a fast linear combination of pairwise overlap (LCPO) algorithm[50] using a probe radius of 1.4 Å.

A common strategy to reduce the noise as well as the computational expense and to cancel errors in simulations is to run molecular dynamics simulations on the complex only. The averages in eq 3 are determined from an ensemble of molecular configurations obtained from such a single trajectory of molecular dynamics simulation. In this single trajectory approach, the covalent energy (E_{cov}) as well as the intramolecular electrostatic and van der Waals energy cancel out in the calculation of ΔG_{bind} which can significantly reduce the noise in most cases.

The MMPBSA.py.MPI script in Amber-11 was used to determine total molecular mechanical energies (E_{gas}), the covalent energy (E_{cov}), as well as the van der Waals (E_{vdW}) and electrostatic (E_{elec}) components. This script performs automatically all of the necessary steps to estimate the binding free energy of protein−ligand complexes using the MM-GBSA method. The electrostatic contribution to the solvation free energy (G_{GB}) was estimated using the generalized Born (GB) model. For the solution of the GB equation, the dielectric constants in the protein and in the water were set to 1 and 80, respectively. The ionic strength was set to 0.15 M. Generally the entropic contribution to the binding free energy is calculated via normal-mode analysis which is a memory intensive and computational expensive method. The formation of macromolecular complexes is in general opposed by a loss in configurational entropy of the binding partners. The configurational entropy is crucial for predicting absolute binding free energies. Since configurational entropies show large fluctuations, a large number of snapshots are required for reliable calculations. In addition, the evaluation of the entropy for such a big system would be very time-consuming and memory intensive. On the other hand, the contribution from the configurational entropy nearly cancels out for relative binding free energies which were the main focus of our work.[35,42,43] The cancellation of the entropic contribution is particularly expected for the current systems. This is because single point mutations do not cause much change to the structure which is supported by the structure 2WOM for the K103N mutant which only shows an rmsd of 0.30 Å for the C_α atoms from the wild-type structure, as we have found. As the entropy thus appeared not to be important in the context of our work and at the same time the determination of the entropy would have been excessively expensive, we did not attempt to do such calculations.

The mutation-induced shift in the binding free energy denoted as relative binding free energy was computed from

$$\Delta\Delta G_{bind} = \Delta G_{mutant} - \Delta G_{wild\ type} \tag{8}$$

Hence, the change in the dissociation constant was evaluated. The dissociation constant in M^{-1} is estimated from the relation $K_d = e^{-\Delta G_{diss}/RT}$ where $\Delta G_{diss} = -\Delta G_{bind}$ and ΔG_{diss} is denoted as dissociation free energy. The dissociation constant K_d for the reaction described in 1 is defined as

$$K_d = \frac{[\mathrm{P}][\mathrm{I}]}{[\mathrm{PI}]} \tag{9}$$

where [X] denotes the concentration of species X. The ratio of the dissociation constants for the RT wild type and the RT mutant, K_d and K'_d, respectively,

$$r \equiv K'_d/K_d \tag{10}$$

was determined from

$$r = \exp(\Delta\Delta G_{bind}/RT) \tag{11}$$

3. RESULTS AND DISCUSSION

To understand the mechanisms underlying the binding of LRV to the wild-type RT and its variants, an energetic analysis using the MM-PB(GB)SA method was conducted. Molecular configurations obtained from MD simulations of the complexes in explicit water were used for the calculation of binding free energies.

dx.doi.org/10.1021/jp300818c | J. Phys. Chem. B 2012, 116, 6269−6278

3.1. Structural Stability. The production simulations of 5 ns carried out for these systems were stable on the basis of the total and potential energies of these systems (data not shown) and the root-mean-square deviation (rmsd) from the X-ray structures. The rmsd's for the backbone atoms from the corresponding X-ray crystal structure in the simulations are shown in Figure 4.

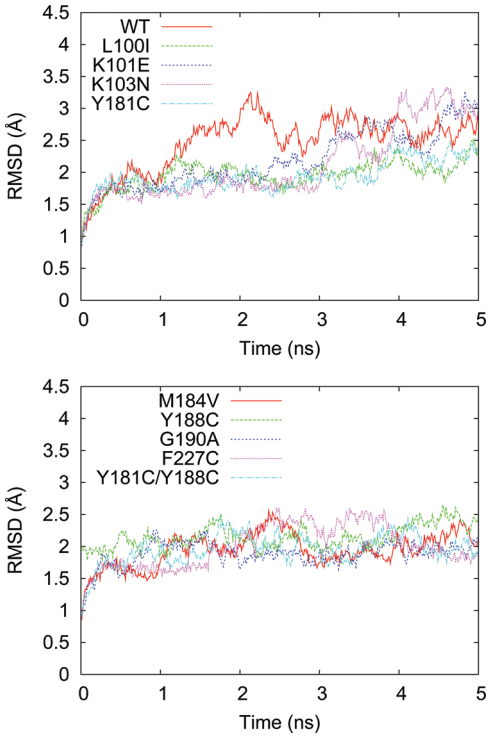

Figure 4. rmsd for the backbone atoms from the corresponding X-ray crystal structures in the simulations.

The average rmsd's for the backbone atoms from the corresponding X-ray crystal structure during the final 3 ns of the simulations were 2.7 (0.2) Å, 2.0 (0.2) Å, 2.5 (0.4) Å, 2.4 (0.5) Å, 2.1 (0.2) Å, 2.1 (0.2) Å, 2.5 (0.4) Å, 1.9 (0.1) Å, and 2.0 (0.2) Å for the RT_{WT}−LRV, RT_{L100I}−LRV, RT_{K101E}−LRV, RT_{K103N}−LRV, RT_{Y181C}−LRV, RT_{M184V}−LRV, RT_{Y188C}−LRV, RT_{G190A}−LRV, and $RT_{Y181C/Y188C}$−LRV complexes, respectively. It is clearly seen from Figure 4 that the rmsd of the RT_{WT}−LRV complex increases during the initial 2 ns of the simulation. After that the rmsd starts decreasing and fluctuates around 2.5 Å. On the other hand, for the K103N mutant complex, the rmsd increases during the initial 500 ps of the simulation and then is stable in the subsequent 3 ns of the simulation. However, after that the rmsd increases slightly and fluctuates around 2.5 Å. The K103N mutant complex is more stable than the WT complex during the initial 3 ns of the simulations. After that both complexes are almost equally stable. For all other mutant complexes, the rmsd increases during the initial 500 ps of the simulation, and after that the rmsd is stable and fluctuates around 2.0 Å.

3.2. Binding Energetics. In our current study, we are interested to evaluate the relative potency of LRV against the wild type and the mutant H IV-1 RT and the molecular basis of drug resistance. The energetics of binding LRV to the wild-type RT and its mutant variants obtained from the MM-GBSA calculations are shown in Table 1. To elucidate the binding mechanisms, we also provide the individual contributions to the binding free energies. Here, the contribution from the van der Waals or electrostatic interactions between the RT and the inhibitor, ΔE_{elec} or ΔE_{vdW}, respectively, and the polar or nonpolar solvation free energy, ΔG_{pol} or G_{np}, correspondingly, were considered. The total binding free energies are found to range between −49 to −52 kcal·mol^{-1}. It is to be noted that this is not an absolute binding free energy since the entropic contribution to the binding is not included. The contributions favoring binding are the van der Waals interaction between the binding partners, being in the range −56.8 to −57.2 kcal·mol^{-1}, and the intermolecular electrostatic energy in the range −15.9 to −22.5 kcal·mol^{-1} for all RT−LRV complexes. The nonpolar interactions with the solvent including the contribution from the hydrophobic effect yield contributions in the range −6.0 kcal·mol^{-1} for LRV complexed with the wild-type and mutant variants of RT. The association is opposed by an unfavorable desolvation of polar groups, yielding a contribution of 28.5 to 32.6 kcal·mol^{-1} for LRV complexed with the wild type and mutant RT. As found for other systems,[26,42] the unfavorable desolvation of polar groups is only partially compensated by favorable intermolecular electrostatic interactions. The sum of the contribution from the desolvation of polar groups and the intermolecular electrostatic interactions varies from 10.1 to 14.2 kcal·mol^{-1} for all RT-inhibitor complexes. The binding mode for LRV complexed with the wild type and the K103N mutant RT is shown in Figure 5.

3.3. Mutation-Induced Change in Binding Affinity. As shown in Table 1, the predicted total binding free energies of the WT, RT_{L100I}, RT_{K101E}, RT_{K103N}, RT_{Y181C}, RT_{M184V}, RT_{Y188C}, RT_{G190A}, RT_{F227C}, and $RT_{Y181C/Y188C}$/LRV complexes using the

Table 1. Free Energy Terms (kcal·mol^{-1}) for the Binding of LRV to the Wild-Type and Mutant Variants of HIV-1 RT[a]

mutant	ΔE_{vdW}	ΔE_{elec}	ΔG_{np}	ΔG_{pol}	ΔG_{solv}[b]	$\Delta G_{pol,elec}$[c]	ΔG_{bond}[d]
WT	−57.2(0.3)	−16.8(0.4)	−5.8(0.01)	29.3(0.3)	23.5(0.3)	12.5(0.5)	−50.5(0.1)
K103N	−56.3(0.2)	−16.4(0.4)	−5.9(0.01)	28.5(0.3)	22.6(0.3)	12.1(0.4)	−50.1(0.1)
L100I	−56.8(0.1)	−15.9(0.2)	−6.0(0.01)	29.4(0.1)	23.4(0.1)	13.5(0.2)	−49.2(0.1)
K101E	−57.3(0.3)	−18.3(0.2)	−5.8(0.01)	32.0(0.3)	26.2(0.3)	13.7(0.4)	−49.4(0.1)
Y181C	−55.8(0.1)	−19.7(0.2)	−5.9(0.01)	31.4(0.1)	25.5(0.1)	11.7(0.2)	−50.0(0.1)
M184V	−57.2(0.1)	−19.9(0.2)	−5.9(0.01)	31.5(0.1)	25.6(0.1)	11.6(0.2)	−51.5(0.1)
Y188C	−56.2(0.1)	−20.0(0.2)	−5.9(0.01)	31.1(0.1)	25.2(0.2)	10.1(0.2)	−50.9(0.1)
G190A	−57.1(0.1)	−19.2(0.2)	−5.9(0.01)	31.3(0.1)	25.4(0.1)	12.1(0.4)	−50.9(0.1)
F227C	−56.5(0.2)	−15.9(0.3)	−5.9(0.01)	30.1(0.2)	24.2(0.2)	14.2(0.4)	−48.2(0.2)
Y181C/Y188C	−56.4(0.1)	−22.5(0.3)	−5.8(0.01)	32.6(0.1)	26.8(0.1)	10.1(0.3)	−52.1(0.2)

[a]Standard errors of the mean are given in parentheses. [b]$\Delta G_{solv} = \Delta G_{np} + \Delta G_{pol}$. [c]$\Delta G_{pol,elec} = \Delta G_{pol} + \Delta E_{elec}$. [d]$\Delta G_{bind} = \Delta E_{vdW} + \Delta E_{elec} + \Delta G_{solv}$.

dx.doi.org/10.1021/jp300818c | J. Phys. Chem. B 2012, 116, 6269−6278

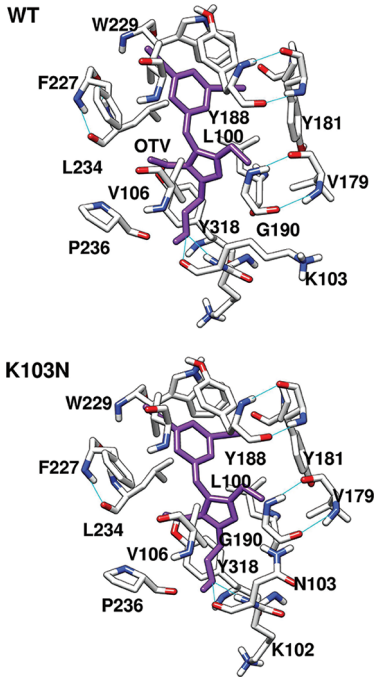

Figure 5. Binding mode of LRV (purple) to RT_{WT} and RT_{K103N}. The protein and the ligand are shown in stick representation. Colors distinguish between oxygen (red), nitrogen (blue), and carbon (white). Hydrogen bonds are depicted as dotted lines.

single trajectory scheme are −50.5 kcal·mol^{-1}, −49.2 kcal·mol^{-1}, −49.4 kcal·mol^{-1}, −50.1 kcal·mol^{-1}, −50.0 kcal·mol^{-1}, −51.5 kcal·mol^{-1}, −50.9 kcal·mol^{-1}, −48.2 kcal·mol^{-1}, and −52.1 kcal·mol^{-1}, respectively. Compared to the WT RT−LRV complex, the mutants RT_{L100I}, RT_{K101E}, RT_{K103N}, RT_{Y181C}, and RT_{F227C} caused a shift of 1.3 kcal·mol^{-1}, 1.1 kcal·mol^{-1}, 0.4 kcal·mol^{-1}, 0.5 kcal·mol^{-1}, and 2.3 kcal·mol^{-1} in the binding free energy, respectively, which suggests that all of these mutants bind less strongly to LRV than the wild type RT. This also implies that the mutations L100I, K101E, K103N, Y181C, and F227C are expected to cause drug resistance against LRV. However, M184V, Y188C, G190A, and Y181C/Y188C do not lead to drug resistance against the inhibitor LRV but cause a significant gain in affinity. Compared to the RT_{WT}−LRV complex, the mutants RT_{M184V}, RT_{G190A}, RT_{Y188C}, and $RT_{Y181C/Y188C}$ caused a gain of 1.0 kcal·mol^{-1}, 0.4 kcal·mol^{-1}, 0.4 kcal·mol^{-1}, and 1.6 kcal·mol^{-1}, respectively, in the size of the binding free energy. This suggests that the inhibitor LRV will be more potent against RT_{M184V}, RT_{G190A}, RT_{Y188C}, and $RT_{Y181C/Y188C}$ compared to the wild type RT, in agreement with the experiment.[9]

From the mutation-induced shift in binding free energy $\Delta\Delta G_{bind}$, the corresponding change in association constants, r, was evaluted. The relative dissociation constants are shown in Table 2.

The K103N or Y181C mutations cause a 2-fold increase in the dissociation constant K_d. The inhibitor thus still retains the potency against these two HIV-1 RT mutants, among which K103N is the most common mutation found in HIV-1 RT. However, the potency is lost in the case of the L100I, the K101E, and the F227C mutant, for which K_d is increased 7-, 9-, and 54-fold, respectively.

On the other hand, no drug resistance is observed for the M184V, Y188C, G190A, and Y181C/Y188C mutants; the inhibitor shows even increased potency against these mutants compared to wild type RT. For these mutations, K_d is decreased, namely, by a factor of 0.5 for the mutants Y181C and G190A, 0.2-fold for M184V, and 0.1-fold for Y181C/188C. The mutation-induced changes in K_d are in agreement with experimental data, also shown in Table 2.

Table 2. Relative Binding Free Energies $\Delta\Delta G_{sim}$ and Relative Dissociation Constants r^{sim} and r^{exp} for HIV-1 RT−LRV Complexes[a]

variant	$\Delta\Delta G_{sim}$[b] (kcal·mol^{-1})	r^{sim}	r^{exp}[a]
K103N	0.4(0.1)	2	∼2
L100I	1.3(0.1)	9	<10
K101E	1.1(0.1)	7	∼8
Y181C	0.5(0.1)	2	∼3
M184V	−1.0(0.1)	0.2	∼0.7
Y188C	−0.4(0.1)	0.5	∼0.8
G190A	−0.4(0.1)	0.5	NA
F227C	2.3(0.2)	54	∼55
Y181C/Y188C	−1.6(0.2)	0.1	∼0.05

[a]Obtained from ref 9. [b]$\Delta\Delta G_{sim} = \Delta G_{MUT} - \Delta G_{WT}$.

L100I Mutant. This mutation causes a 1.3 kcal·mol^{-1} change in the binding free energy compared to the wild type which can be seen from Table 2. The electrostatic and van der Waals interaction energy is shifted by 0.9 kcal·mol^{-1} and 0.4 kcal·mol^{-1}, respectively. Hence, drug resistance arises mainly due to the loss in the size of the intermolecular electrostatic energy.

K101E Mutant. The van der Waals interaction energy ΔE_{vdW} remains almost unaffected by the K101E mutation. The electrostatic energy ΔE_{elec} is shifted by −1.5 kcal·mol^{-1}, but the polar solvation free energy is increased by 2.7 kcal·mol^{-1}. Thus, the change in ΔE_{elec} is not sufficient to counter the increase in ΔG_{pol}, being the origin of the drug resistance.

K103N Mutant. Our calculations show that LRV retains activity against this key NNRTI-resistant mutation for which only a 2-fold increase in the dissociation constant is observed. In contrast, the same mutation causes an almost 60-fold increase in the dissociation constant of RT_{K103N}-efavirenz.[9] The change in ΔE_{elec} and ΔE_{vdW} is 0.4 kcal·mol^{-1} and 0.9 kcal·mol^{-1}, respectively. However, this is almost compensated by a shift in the polar solvation free energy by −0.8 kcal·mol^{-1}. Hence, only a 2-fold increase in the dissociation constant is observed for this key mutant, in agreement with experimental results.[9] The binding of LRV to WT and the K103N mutant is shown in Figure 5.

Y181C Mutant. The Y181C mutation induces a 2-fold decrease in the dissociation constant. The mutation causes a change in ΔE_{vdW} by 1.4 kcal·mol^{-1}, while ΔE_{elec} is shifted by −2.9 kcal·mol^{-1} compared to the wild type. The desolvation free energy ΔG_{pol} is increased by 2.1 kcal·mol^{-1}. Thus, the increased size of ΔE_{elec} partially counter balances the loss in the magnitude of ΔE_{vdW} and the gain in ΔG_{pol}, which is the reason why only a slight increase in the dissociation constant is found.

M184V Mutant. The M184V mutant causes no drug resistance. Rather, our calculation shows that LRV is more potent against this mutant compared to the wild type RT. The change in ΔG due to this mutation is −1.0 kcal·mol^{-1}. There is no change in ΔE_{vdW} compared to the wild type for this mutant. However, this mutation causes a shift in ΔE_{elec} by −3.1 kcal·mol^{-1}. This change in ΔE_{elec} is partially counter balanced due to an increase in ΔG_{pol} by 2.2 kcal·mol^{-1}. This leads to an

dx.doi.org/10.1021/jp300818c | J. Phys. Chem. B 2012, 116, 6269−6278

overall increase in the size of the binding free energy for this mutant. In this case, the gain in binding affinity arises from the change in the intermolecular electrostatic energy which, thus, is the origin of the increase in potency.

Y188C and G190A Mutants. Both mutants cause an increase in the size of the binding free energy. Hence, no drug resistance arises in these two cases; rather, LRV is more potent against these two mutants compared to the wild type. We observe a change in ΔE_{vdW} by 1.0 kcal·mol^{-1} for the Y188C mutant, while almost no change in ΔE_{vdW} is observed for the G190A mutant. The electrostatic energy is shifted by around −3.1 kcal·mol^{-1} for both mutants, while the unfavorable polar solvation free energy for both cases is increased by about 2 kcal·mol^{-1} compared to the wild type. The gain in the binding affinity hence arises from the change in the intermolecular electrostatic interactions.

F227C Mutant. This mutation provides significant drug resistance. The change in binding free energy is 2.4 kcal·mol^{-1} which translates to a 54-fold increase in the dissociation constant. The changes in ΔE_{vdW}, ΔE_{elec}, and ΔG_{pol} are all around 0.8 ± 0.1 kcal·mol^{-1} and, hence, equally contribute to the drug resistance. The shift in ΔE_{elec} correlates well with a disruption of the hydrogen bonding between the drug and the K103 residue visible in Figure 6.

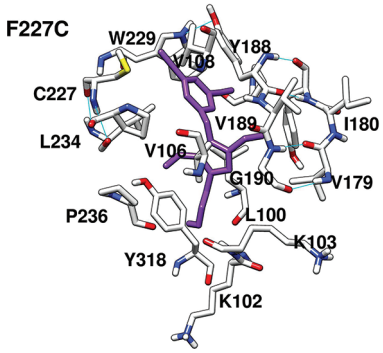

Figure 6. Binding of LRV (purple) to RT$_{F227C}$. The representation is similar to that chosen in Figure 5.

Y181C/Y188C Mutant. Our calculations show that Y181C causes drug resistance while LRV appears to be more potent against the Y188C mutant compared to the wild type. When these two mutations occur at the same time, we observe a significant shift in the binding free energy compared to the wild type by −1.6 kcal·mol^{-1}. This gain in binding free energy is intermolecular electrostatics driven which can be seen from Table 1. The intermolecular electrostatic energy is changed by −5.7 kcal·mol^{-1}, whereas the polar component of the solvation free energy is increased by 3.3 kcal·mol^{-1} and the van der Waals interaction energy is shifted by 0.8 kcal·mol^{-1}. The total change in ΔE_{vdW} and ΔG_{pol} is thus not enough to counter balance the shift in the electrostatic energy ΔE_{elec} which, thus, is the origin of the increase in binding affinity.

3.4. Interaction Energies for Individual Residues. The binding free energies were further decomposed into contributions from each RT residue. The decomposition of the energy was conducted on a pairwise per-residue basis, in which the interactions included the contributions from side chains and the backbone of the residues. The RT-inhibitor interaction spectra for the WT, K103N, Y181C, and G190A cases are shown in Figure 7. It is clear from the figure that, overall, the interaction spectra of all of the complexes are quite similar.

Energetic components from the interactions between LRV and the important residues of the wild type and mutant RT are summarized in Table 3. The decomposition shows that the main contributions are −3.04 kcal·mol^{-1} and −3.52 kcal·mol^{-1} from Leu100 and Tyr188, respectively, in the RT$_{WT}$−LRV complex. Similarly, for all of the mutant variants, the main contributions are coming from Leu100 and Tyr188. A similar trend was observed for the RT−nevirapine complex in a previous study.[2]

Our results are also in agreement with experimental findings. Structural inspection[9] suggests that V108 forms extensive van der Waals interactions with the dicyano-substituted phenol moiety of LRV, which forms three hydrogen bonds with the backbone of Lys103 and Pro236, as well as interactions with residues L100, V106, Y181C, Y188, F227, W229, L234, P236, and Y318 of the p66 subunit of RT. Our calculations facilitate to quantify and rank these interactions. We find that the sizes of the interactions decrease in the order Y188 (−3.52 kcal·mol^{-1}), Y188 (−3.52 kcal·mol^{-1}), L100 (−3.04 kcal·mol^{-1}), V106 (−2.24 kcal·mol^{-1}), Y318 (−1.92 kcal·mol^{-1}), W229 (−1.88 kcal·mol^{-1}), L234 (−1.81 kcal·mol^{-1}), F227 (−1.52 kcal·mol^{-1}), Y181 (−0.98 kcal·mol^{-1}), K103 (−0.88), and P236 (−0.71 kcal·mol^{-1}).

L100I and K101E Mutant. For the L100I mutant, the sizes of the contributions from I100 and W229 are decreased by 0.34 kcal·mol^{-1} and 0.41 kcal·mol^{-1}, respectively, leading to the drug resistance. Contributions from other residues do not change much for the L100I mutant. For the K101E mutant, a significant drop in the size of the contribution is observed for residues K102 (0.53 kcal·mol^{-1}), K103 (0.31 kcal·mol^{-1}), and P236 (0.34 kcal·mol^{-1}).

K103N Mutant. When K103 is replaced by N103, the contribution from this particular residue is shifted by −0.44 kcal·mol^{-1}. A favorable change (by −0.34 kcal·mol^{-1}) is also observed for the contribution from residue P236. However, the size of the contribution from K102 and W229 are decreased by 0.91 kcal·mol^{-1} and 0.24 kcal·mol^{-1}, respectively. Hence the drop in the contribution from residue K102 by 0.91 kcal·mol^{-1} is the main origin of the slight drug resistance for the K103N mutant.

Y181C Mutant. When Tyr at position 181 is replaced by Cys, the contribution to the free energy from this residue is shifted by 0.19 kcal·mol^{-1}. Contributions from K102 and Y318 are decreased in size by 0.21 and 0.37 kcal·mol^{-1}, respectively. However, the contributions from K103 and P236 are shifted by −0.25 kcal·mol^{-1} and −0.60 kcal·mol^{-1}, respectively. The change in the contributions from other residues is within ±0.1 kcal·mol^{-1}.

M184V Mutant. For this mutant, the contributions from residues L100, K103, W229, L234, and P236 are increased in size. In particular, a notable effect is seen for the residue P236 whose contribution shows a shift of −0.61 kcal·mol^{-1}. For the other residues, the magnitude of the corresponding contributions is decreased. A significant drop of ∼0.3 kcal·mol^{-1} in the ligand-residue interaction energies is observed for K101 and Y318.

Y188C Mutant. This mutation causes a decrease in the size of the interaction energies for L100, V106, V108, Y181, Y188, and Y318. Among those, the shift is clearly largest for the residue Y318 (0.3 kcal·mol^{-1}). For other residues, an increase in the magnitude of the interaction energies is observed. Here

dx.doi.org/10.1021/jp300818c | J. Phys. Chem. B 2012, 116, 6269−6278

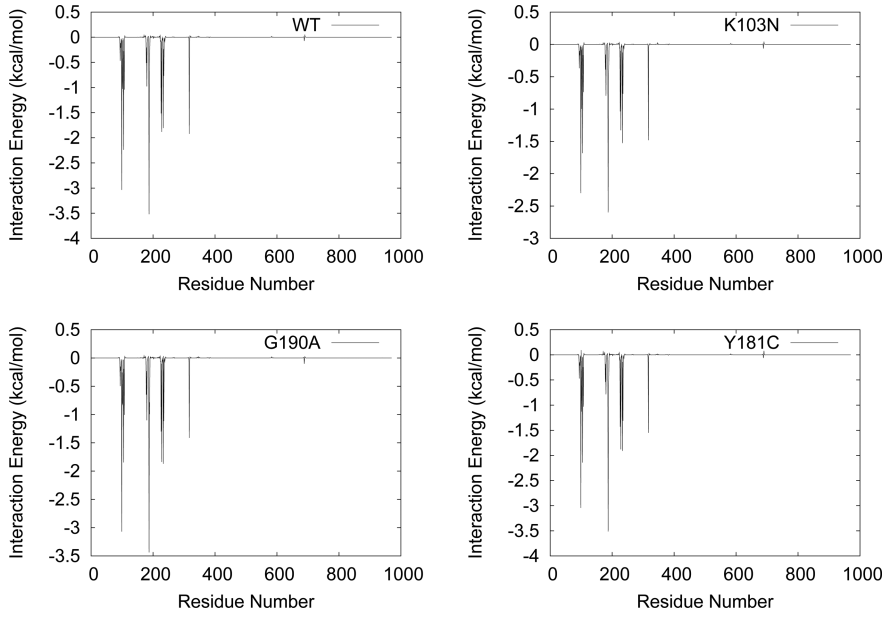

Figure 7. Decomposition of the binding free energies for the RT-inhibitor complex into contributions from individual residues.

Table 3. Decomposition of Binding Free Energies for RT−LRV into Contributions from the Most Important Residues[a]

residue	WT	L100I	K101E	K103N	Y181C	M184V	Y188C	G190A	F227C	DM[b]
L100I	−3.04	−2.70	−2.99	−3.02	−3.04	−3.10	−2.95	−3.07	−2.92	−2.89
K102	−1.03	−1.02	−0.50	−0.12	−0.82	−0.73	−1.10	−0.78	−0.16	−0.92
K103N	−0.88	−0.88	−0.57	−1.32	−1.13	−1.08	−0.98	−0.90	−0.81	−1.23
V106	−2.24	−2.15	−2.31	−2.13	−2.14	−2.11	−2.13	−1.75	−2.22	−2.07
V108	−1.04	−0.89	−0.97	−1.02	−1.03	−1.01	−0.98	−1.03	−0.94	−0.98
Y181C	−0.98	−1.21	−1.21	−1.10	−0.79	−1.19	−0.81	−1.10	−1.19	−0.88
Y188C	−3.52	−3.51	−3.37	−3.38	−3.51	−3.50	−3.48	−3.49	−3.52	−3.56
F227C	−1.52	−1.28	−1.74	−1.34	−1.43	−1.48	−1.55	−1.44	−0.57	−1.41
W229	−1.88	−1.47	−2.05	−1.64	−1.88	−1.95	−1.98	−1.94	−1.95	−1.94
L234	−1.81	−1.92	−1.84	−1.92	−1.91	−1.87	−1.83	−1.91	−1.81	−1.82
P236	−0.71	−0.70	−0.47	−1.05	−1.31	−1.31	−1.44	−1.06	−1.19	−1.20
Y318	−1.92	−1.85	−1.87	−1.99	−1.55	−1.63	−1.62	−1.59	−1.86	−1.80

[a]All values are given in kcal·mol^{-1}. [b]DM ≡ Y181C/Y188C.

the most favorable shift (−0.73 kcal·mol^{-1}) is seen for the residue P236. The increase in the interaction energy for P236 is mainly responsible for the overall increase in size of the binding free energy compared to the wild type.

G190A Mutant. When glycine at position 190 is replaced by alanine, the total binding free energy is increased in the size compared to the wild type. This gain in the size of the binding free energy corresponds to an increase in the magnitude of the interaction energies of residues L100, K103, Y181, W229, L234, and P236. A significant increase in the magnitude of the interaction energy is observed only for the P236 residue which shows a shift of −0.35 kcal·mol^{-1}. A slight increase in the size of the interaction energy is found for the residues L100, K103, Y181, W229, and L234. The interaction energies for the remaining residues in Table 3 decreased in magnitude, and significant shifts are observed for K102 (0.25 kcal·mol^{-1}), V106 (0.45 kcal·mol^{-1}), and Y318 (0.33 kcal·mol^{-1}).

F227C Mutant. When F227 is replaced by the amino acid C, the size of the interaction energy for this particular residue drops by 0.97 kcal·mol^{-1}. Likewise, the contribution from K102 decreases by 0.86 kcal·mol^{-1} in magnitude. On the other hand, the size of the contribution from P236 is increased by −0.47 kcal·mol^{-1}. Drug resistance mainly arises due to the loss in interaction energy from residues C227 and K102.

Y181C/Y188C. This double mutation causes a slight decrease in the interaction energy for C181 (0.1 kcal·mol^{-1}) and a negligible shift for residue C188 (−0.04 kcal·mol^{-1}). However, significant favorable shifts are observed for the contributions from P236 (−0.49 kcal·mol^{-1}) and K103 (−0.35 kcal·mol^{-1}), which lead to the stronger binding of LRV to this double mutant compared to the wild type.

4. CONCLUSION

In our current work, we study the potency of a newly synthesized nonnucleoside reverse transcriptase inhibitor (NNRTI), lersivirine (UK-453061), against wild-type and drug-resistive mutant variants of the RT using molecular dynamics simulations and free energy calculations. The well-established and popular molecular mechanics-generalized Born (MM-GBSA) method was used to estimate the components of the binding free energy. Our calculation suggests that the binding of LRV to RT is largely driven by the van der Waals (E_{vdW}) interactions between LRV and RT. Also the intermolecular electrostatic interactions and the nonpolar

dx.doi.org/10.1021/jp300818c | J. Phys. Chem. B 2012, 116, 6269−6278

component of the solvation free energy contribute favorably to the binding of LRV to HIV-1 RT. Furthermore, we have investigated the drug resistance of LRV against eight single mutations and one double mutation in HIV-1 RT. Our study shows that the L100I, K101E, K103N, Y181C, and F227C mutations cause drug resistance. It is remarkable, though, that the dissociation constant K_d is increased at most a 10-fold decrease except for the case of F227C which causes a 54-fold increase in the dissociation constant. Especially, K_d is only increased 2-fold for the K103N and the Y181C mutants, due to a balance of opposite changes in the polar solvation as well as the electrostatic and van der Waals interactions between LRV and RT. The dissociation constant is even decreased for the Y188C and G190A (2-fold), the M184V (5-fold), and the Y188C/Y188C mutant (10-fold), due to stronger electrostatic interactions between LRV and RT compared to wild type RT. This means that the inhibitor LRV will be more potent against such mutations compared to the wild type RT in agreement with experiments. Overall, our calculations suggest that LRV is a potent NNRTI which retains its activity against many drug resistant mutations, in agreement with experimental results, and reveal important factors for LRV's potency.

■ ASSOCIATED CONTENT

Supporting Information

The rmsd for the backbone atoms from the corresponding X-ray crystal structures in the simulations. This material is available free of charge via the Internet at http://pubs.acs.org.

■ AUTHOR INFORMATION

Corresponding Author

*E-mail: Volker.Knecht@mpikg.mpg.de. Phone: +49-331-567-9732. Fax: +49-331-567-9612.

Notes

The authors declare no competing financial interest.

■ ACKNOWLEDGMENTS

This work was partly supported by the Federal Ministry of Education and Research (BMBF), Germany. P.K. acknowledges the support from the International Research Training Group 1524.

■ REFERENCES

(1) *UNAIDS publication series*; UNAIDS: Geneva, 2009.
(2) Treesuwan, W.; Hannongbua, S. *J. Mol. Graphics Modell.* **2009**, *27*, 921−929.
(3) Whitcomb, J. M.; Hughes, S. H. *Annu. Rev. Cell Biol.* **1992**, *8*, 275−306.
(4) Kohlstaedt, L. A.; Wang, J.; Friedman, J. M.; Rice, P. A.; Steitz, T. A. *Science* **1992**, *256*, 1783−1790.
(5) de Béthune, M.-P. *Antiviral Res.* **2009**, *85*, 75−90.
(6) Huang, H.; Chopra, R.; Verdine, G. L.; Harrison, S. C. *Science* **1998**, *282*, 1669−1675.
(7) Wood, E.; Hogg, R. S.; Yip, B.; Moore, D.; Harringan, P. R.; Montaner, J. S. *HIV Med.* **2007**, *8*, 80−85.
(8) Walker, B. D.; Burton, D. R. *Science* **2008**, *320*, 760−764.
(9) Corbau, R.; Mori, J.; Phillips, C.; Fishburn, L.; Martin, A.; Mowbray, C.; Panton, W.; Smith-Burchnell, C.; Thornberry, A.; Ringrose, H.; et al. *Antimicrob. Agents Chemother.* **2010**, *54*, 4451−4463.
(10) Baba, M.; Tanaka, H.; de Clercq, E.; Pauwels, R.; Balzarini, J.; Schols, D.; Nakashima, H.; Perno, C. F.; Walker, R. T.; Miyasaka, T. *Biochem. Biophys. Res. Commun.* **1989**, *165*, 1375−1381.
(11) Pauwels, R.; Andries, K.; Desmyter, J.; Schols, D.; Kukla, M. J.; Breslin, H. J.; Raeymaeckers, A.; van Gelder, J.; Woestenborghs, R.; Heykants, J. *Nature* **1990**, *343*, 470−474.
(12) Merluzzi, V. J.; Hargrave, K. D.; Labadia, M.; Grozinger, M.; Skoog, M.; Wu, J. C.; Shih, C. K.; Eckner, K.; Hattox, S.; Adams, J. *Science* **1990**, *250*, 1411−1413.
(13) Young, S. D.; Britcher, S. F.; Tran, L. O.; Payne, L. S.; Lumma, W. C.; Lyle, T. A.; Huff, J. R.; Anderson, P. S.; Olsen, D. B.; Carroll, S. S. *Antimicrob. Agents Chemother.* **1995**, *39*, 2602−2605.
(14) Freimuth, W. W. *Adv. Exp. Med. Biol.* **1996**, *394*, 279−289.
(15) Tantilo, C.; Ding, J.; Jacobo-Molina, A.; Nanni, R. G.; Boyer, P. L.; Hughes, S. H.; Pauwels, R.; Andries, K.; Janssen, P. A. J.; Arnold, E. *J. Mol. Biol.* **1994**, *243*, 369−387.
(16) Esnouf, R.; Ren, J.; Ross, C.; Jones, Y.; Stammers, D.; Stuart, D. *Nat. Struct. Biol.* **1995**, *2*, 303−308.
(17) Soriano, V.; de Mendoza, C. *HIV Clin. Trials* **2002**, *3*, 237−248.
(18) Zwanzig, R. W. *J. Chem. Phys.* **1954**, *22*, 1420−1426.
(19) Kirkwood, J. G. *J. Chem. Phys.* **1935**, *3*, 300−313.
(20) Jayaram, B.; Sprous, D.; Young, M. A.; Beveridge, D. L. *J. Am. Chem. Soc.* **1998**, *120*, 10629−10633.
(21) Vorobjev, Y. N.; Almagro, J. C.; Hermans, J. *Proteins* **1998**, *32*, 399−413.
(22) Kollman, P. A.; Massova, I.; Reyes, C.; Kuhn, B.; Huo, S.; Chong, L.; Lee, M.; Lee, T.; Duan, Y.; Wang, W.; et al. *Acc. Chem. Res.* **2000**, *33*, 889−897.
(23) Onufriev, A.; Bashford, D.; Case, D. A. *J. Phys. Chem. B* **2000**, *104*, 3712−3720.
(24) Onufriev, A.; Bashford, D.; Case, D. A. *Proteins* **2004**, *55*, 383−394.
(25) Hou, T.; Wang, J.; Li, Y.; Wang, W. *J. Chem. Inf. Model* **2011**, *51*, 69−82.
(26) Kuhn, B.; Kollman, P. A. *J. Med. Chem.* **2000**, *43*, 3786−3793.
(27) Rastelli, G.; Rio, A. D.; Degliesposti, G.; Sgobba, M. *J. Comput. Chem.* **2010**, *31*, 797−810.
(28) Reyes, C. M.; Kollman, P. A. *J. Mol. Biol.* **2006**, *295*, 1−6.
(29) Reyes, C. M.; Kollman, P. A. *J. Mol. Biol.* **2000**, *297*, 1145−1158.
(30) Wang, J.; Morin, P.; Wang, W.; Kollman, P. A. *J. Am. Chem. Soc.* **2001**, *123*, 5221−5230.
(31) Worch, R.; Bökel, C.; Höfinger, S.; Schwille, P.; Weidemann, T. *Proteomics* **2010**, *10*, 4196−4208.
(32) Kar, P.; Seel, M.; Weidemann, T.; Höfinger, S. *FEBS Lett.* **2009**, *583*, 1909−1915.
(33) Karplus, M.; Kushick, J. N. *Macromolecules* **1981**, *14*, 325−332.
(34) Rempe, S. B.; Jonsson, H. *Chem. Educ.* **1998**, *3*, 1−17.
(35) Massova, I.; Kollman, P. A. *J. Am. Chem. Soc.* **1999**, *36*, 8133−8143.
(36) Hornak, V.; Abel, R.; Okur, A.; Strockbine, B.; Roitberg, A.; Simmerling, C. *Proteins* **2006**, *65*, 712−725.
(37) Wang, J.; Wolf, R. M.; Caldwell, J. W.; Kollman, P. A.; Case, D. A. *J. Comput. Chem.* **2004**, *25*, 1157−1174.
(38) Jakalian, A.; Jack, D. B.; Bayly, C. I. *J. Comput. Chem.* **2002**, *23*, 1623−1641.
(39) Wang, J.; Wang, W.; Kollman, P. A.; Case, D. A. *J. Mol. Graphics Modell.* **2006**, *25*, 247−260.
(40) Case, D. A.; Cheatham, T.; Darden, T.; Gohlke, H.; Luo, R.; Merz, K. M., Jr.; Onufriev, A.; Simmerling, C.; Wang, B.; Woods, R. *J. Comput. Chem.* **2005**, *26*, 1668−1688.
(41) Dewar, M. J. S.; Zoebisch, E. G.; Healy, E. F.; Stewart, J. J. P. *J. Am. Chem. Soc.* **1985**, *107*, 3902−3909.
(42) Kar, P.; Lipowsky, R.; Knecht, V. *J. Phys. Chem. B* **2011**, *115*, 7661−7669.
(43) Kar, P.; Knecht, V. *J. Comput. Aided Mol. Des.* **2012**, *26*, 215−232.
(44) Kar, P.; Knecht, V. *J. Phys. Chem. B* **2012**, *116*, 2605−2614.
(45) Kar, P.; Knecht, V. *J. Phys. Chem. B*; DOI: 10.1021/jp3022612.
(46) Jorgensen, W. L.; Chandrasekar, J.; Madura, J. D.; Impey, R.; Klein, K. *J. Chem. Phys.* **1983**, *79*, 926−935.
(47) Ryckaert, J.-P.; Ciccotti, G.; Berendsen, H. J. C. *J. Comput. Phys.* **1977**, *23*, 327−341.

(48) Darden, T.; York, D.; Pedersen, L. *J. Chem. Phys.* **1993**, *98*, 10089−10092.
(49) Sitkoff, D.; Sharp, K. A.; Honig, B. *J. Phys. Chem.* **1994**, *98*, 1978−1988.
(50) Weise, J.; Shenkin, P. S.; Still, W. C. *J. Comput. Chem.* **1999**, *20*, 217−230.